Naval Research Laboratory

Washington, DC 20375-5320

NRL/MR/7620--95-7737

The SPARTAN 1 Collimated X-Ray Detector System

G.G. FRITZ
R.G. CRUDDACE
M.P. KOWALSKI
W.A. SNYDER
R.M. TAIT
D.W. WOODS

X-Ray Astronomy Branch
Space Science Division

E.E. FENIMORE
E. SERNA
J. MIDDLEDITCH

Los Alamos National Laboratory
Los Alamos, New Mexico

M.P. ULMER

Northwestern University
Evanston, Illinois

August 7, 1995

REPORT DOCUMENTATION PAGE

Form Approved
OMB No. 0704-0188

1. AGENCY USE ONLY (*Leave Blank*)	2. REPORT DATE	3. REPORT TYPE AND DATES COVERED
	August 7, 1995	Memorandum Report

4. TITLE AND SUBTITLE

The Spartan 1 Collimated X-Ray Detector System

5. FUNDING NUMBERS

6. AUTHOR(S)

G.G. Fritz, E.E. Fenimore,* M.P. Ulmer,** R.G. Cruddace, E. Serna,* J. Middleditch,* M.P. Kowalski, W.A. Snyder, R.M. Tait, and D.W. Woods

7. PERFORMING ORGANIZATION NAME(S) AND ADDRESS(ES)

Naval Research Laboratory
Washington, DC 20375-5320

8. PERFORMING ORGANIZATION REPORT NUMBER

NRL/MR/7620--95-7737

9. SPONSORING/MONITORING AGENCY NAME(S) AND ADDRESS(ES)

Office of Naval Research
Arlington, VA 22217

10. SPONSORING/MONITORING AGENCY REPORT NUMBER

11. SUPPLEMENTARY NOTES

*Los Alamos National Laboratory, Los Alamos, New Mexico
**Northwestern University, Evanston, Illinois

12a. DISTRIBUTION/AVAILABILITY STATEMENT

Approved for public release; distribution unlimited.

12b. DISTRIBUTION CODE

13. ABSTRACT (*Maximum 200 words*)

This memorandum documents the design testing and flight performance of the finely collimated x-ray detector system flown on the SPARTAN 1 mission. The SPARTAN program, an outgrowth of a joint Naval Research Laboratory (NRL)/National Aeronautics and Space Administration (NASA) — Goddard Space Flight Center (GSFC) development effort, was instituted by NASA as a means of launching autonomous, recoverable, pointed space science payloads from the shuttle. SPARTAN 1, carrying an NRL x-ray astronomy instrument, was launched by the orbiter Discovery (STS-51G) on June 20, 1985 and recovered 45 hours later on June 22. The instrument, designed to provide both good spatial and spectral resolution, comprised two large proportional counters, an outgrowth of the NRL sounding rocket program, equipped with fine collimators. They provided an effective collecting area of 660 cm^2, a photon energy range of 1-12 keV, and a field of view 5 arc minutes wide (FWHM) and 3 degrees long. The precise pointing of the SPARTAN 1 payload was calibrated by two 35 mm cameras, developed at NRL, which were coaligned with the collimator assembly. The mission was highly successful and yielded spectrally resolved x-ray images of the Perseus cluster of galaxies and the galactic center.

14. SUBJECT TERMS

Astronomy Instrumentation
X-rays
Detectors

15. NUMBER OF PAGES

31

16. PRICE CODE

17. SECURITY CLASSIFICATION OF REPORT	18. SECURITY CLASSIFICATION OF THIS PAGE	19. SECURITY CLASSIFICATION OF ABSTRACT	20. LIMITATION OF ABSTRACT
UNCLASSIFIED	UNCLASSIFIED	UNCLASSIFIED	UL

CONTENTS

The SPARTAN 1 Collimated X-ray Detector System

1 Introduction

In a companion paper (Cruddace et al. 1989) we have described the NASA SPARTAN 1 mission, in which a free-flying payload was launched from the space shuttle orbiter Discovery in June 1985 and then recovered two days later (Figure 1). Its goal was to make X-ray observations of two astrophysical sources, the Perseus cluster of galaxies and the center of our Galaxy. For this purpose it was equipped with two finely collimated proportional counters, and during the mission these detectors scanned the two X-ray sources in a systematic manner. In this report a technical description of the instrument and its operation is given.

We describe first the configuration of the detector assembly and its method of operation during the astrophysical observations. This is followed by a section describing the astrophysical pointing program and the method by which the instrument orientation during the mission was determined precisely. The fourth section contains a technical description of the detectors and their calibration, and in particular the in-orbit calibration. Finally, we provide a careful account of the procedures by which the instrument background count-rates were deduced, as accurate knowledge of these rates is important for the scientific analysis of the data.

2 Configuration and Method of Operation of the Detector Assembly

The complete instrument is shown in Figure 2. It comprises two large proportional counters, each equipped with two fine-collimator modules, and two 35 mm aspect cameras, which are all mounted and co-aligned accurately on a flat rectangular structure (about 1 m square) called the 'optical bench'. The detectors and aspect cameras had to be co-aligned accurately with the SPARTAN 1 attitude control system (ACS), and therefore the ACS startracker and rate-gyros were mounted on the bench also (Figure 2). The mass of the optical bench after assembly was approximately 150 kg.

Manuscript approved May 17, 1995.

The collimators provided each counter with a slit-like field of view (Figure 2b), nominally 5′ wide (full width at half maximum or FWHM) and 3° long (FWHM). The two detectors were to have been co-aligned precisely, but practical considerations made it preferable to leave a residual misalignment of a few arcminutes. As the data from each detector were timed and stored separately in the payload data system, this alignment could be compensated in a straightforward manner during the data analysis. The method of observation was for the ACS to move this slit at a slow rate ($\sim 15 - 20$ arcmin min^{-1}) across the X-ray source in a direction perpendicular to the long axis. The optical bench was fixed in the SPARTAN 1 structure, so that the whole payload functioned as a three-dimensionally stabilized telescope. Each scan yielded a one-dimensional profile of the spatial structure of the X-ray source, and by means of a program of scans in many different directions the two-dimensional structure could be constructed after the flight. The method of construction uses techniques similar to those used in X-ray tomography.

The observations were organized in such a way that the same basic sequence of operations, summarized in the sketch shown in Figure 3, was repeated during each orbit made by SPARTAN 1 around the Earth. Only the orientation of the scan upon the sky changed from orbit to orbit. As indicated in Figure 3, ACS startracker observations of bright stars ('stellar updates') were made each orbit in order to compensate drift of the gyros. The track of the center of the field of view was calibrated in flight by the 35 mm cameras, which made 10 short exposures of the star field during each 'scan sequence'. A scan sequence commenced at the center of the X-ray source, moved out to between 45′ and 60′ from the center, reversed direction to scan through the center out to an equal distance on the other side, and then returned to the center. Figure 3 shows how one scan sequence was employed per orbit for the Galactic center observations, whereas two per orbit were planned for the Perseus cluster.

In addition to the X-ray observations and the stellar updates, measures were taken to calibrate the X-ray detectors in orbit. Although the angular response function of each collimator and its alignment with respect to the startracker were carefully measured before flight, the final calibrations were performed in orbit in order to search for any changes induced by the mechanical and acoustic forces produced during launch or by the thermal conditions encountered during orbital flight. Therefore two slow scans over the strong stellar X-ray source Sco X-2 (1H1702-363) were substituted for the first Galactic center scan sequence. In addition the gain of each detector was calibrated during each orbit in order to monitor slow drifts during the mission. Simultaneous with the stellar update (Figure 3) each X-ray detector was calibrated by shining an ^{55}Fe source of 5.898 keV X-rays into the aperture. In this way small drifts in the detector gain during the mission could be measured.

3 Determination of the Instrument Orientation

The two aspect cameras were designed and built at NRL, and were based on a camera developed for the Apollo 16 Ultraviolet Telescope. Each camera used a Schneider Tele-Xenar f/4.0 lens of focal length 150 mm and contained a film magazine holding 30 ft of Kodak 2475 high-speed recording film. The dimensions of each frame were 18×24 mm, corresponding to

a field of view of $7° \times 9°$. The exposure time, determined by a mechanical shutter, was 10 s, and this sufficed for detection of stars as faint as seventh magnitude. Fiducial lights in the camera impressed images on the film, providing a reference frame for the stellar images which was fixed with respect to the optical bench. Figure 4 shows the trails of the stars during a typical 10 s exposure, and near the corners the images of the four fiducial lights are visible. In one orbit each camera exposed twenty frames during the Perseus observation, ten during the Galactic center observation, and one after the ACS locked on to the star Deneb (α Cyg). The preprogrammed sequence of frames was timed by recording the shutter operation and storing the corresponding times in the payload data. We deal first with observations of the Galactic center and then with the Perseus cluster observations. Aspect camera problems were encountered during the latter, and special data reduction measures were necessary.

The film was analyzed using a measuring machine at the Fermilab, University of Chicago. The positions of the fiducial lights and a sample of about 10 stars were measured on each frame and recorded on magnetic tape. During the stellar update, the stellar images were point-like and therefore easy to measure, but during a slow scan a star trail trail was produced (Figure 4). However the center of each star trail could be measured accurately, and the corresponding time could be determined precisely using the shutter monitor. During analysis of this data the positions on the film were fitted to the known celestial positions of the stars in order to derive the scaling factor and the celestial position of the payload view axis. The latter was defined to be the startracker optical axis, and its position in the reference frame of the fiducial lights was determined from the camera frame obtained while the ACS was locked onto the update star Deneb. It remained to calibrate the relative alignment of the X-ray axis with the startracker axis, and this was performed during the transit of the X-ray star Sco X-2 (see §4.2 below), whose position is known with high precision.

For each scan a great-circle path at a uniform scan rate was fitted to the data, and the results yielded the scan rate and the standard deviations of the measured position both along and perpendicular to the scan path. The results showed that the directions of the scans, which are shown in Figure 5, were very close to the planned orientations, and that the scan rate was remarkably uniform. The results are summarized in Table 1, in which we give also the maximum excursions (peak-to-peak) of the yaw (scan direction) gyro position, as obtained from in-flight gyroscope data. As the fluctuations in the ACS data are noticeably less than the aspect camera solution uncertainties, we conclude that the latter were generated mainly during reading of the film and analysis of the resulting data. The 1σ uncertainties in the position along the scan path and in the scan-rate are ± 0.27 arcmin and ± 0.23 arcmin min^{-1} respectively.

During the Perseus cluster observations, which had to be performed while the target was about 45° from the Sun, the combination of the payload sunshade (Figure 1) and the individual aspect camera sunshades was insufficient to prevent scattered light from fogging the film during the 10 s exposure. The results are illustrated in Figure 6, which shows slices taken from seven consecutive frames in a scan. These slices show the image of the only star which could be detected, Algol (β Per). As the degree of fogging changed from orbit to orbit, because the roll attitude of SPARTAN 1 with respect to the Sun changed, on only

Table 1. Mean scan-rates, and uncertainties in positions and scan-rates, obtained from the aspect camera measurements during the Galactic Center Observation. Also shown are yaw position uncertainties derived from scrutiny of the attitude control system (ACS) housekeeping data. Pitch and roll position errors were of similar magnitude.

Planned scan-rate arcmin min^{-1}	Measured scan-rate (1) arcmin min^{-1}	Yaw error (2) arcmin	ACS yaw error (3) arcmin	Pitch error (4) arcmin
23.20	23.29±0.23	0.27	0.36±0.06	0.34

NOTES

1. The uncertainties are calculated from orbit-to-orbit variations, and they are predominantly measuring errors.
2. Yaw motions are along the scan track.
3. An average over those scans producing satisfactory X-ray data. Seven of the 24 scans were not used because the X-ray data was corrupted in the South Atlantic Anomaly (SAA) by particle events. On one orbit the ACS performance was influenced significantly by the SAA, and the ACS yaw error reached levels five times the normal value.
4. Pitch motions are orthogonal to the scan track.

three scans could Algol be identified by eye on individual frames. However, as the Galactic center observations showed, the scans were being performed at a highly uniform rate and at orientations very close to the planned values, and these two conditions made it possible to extract an attitude solution from these fogged camera frames by means of microdensitometry of the film. The analysis of the X-ray data is sensitive predominantly to errors in position measured along the scan, and small uncertainties in scan orientation are unimportant.

The first step was to measure the scan-rate, using the three orbits in which Algol could be detected on individual frames, which yielded the result 16.2 arcmin min^{-1}. Then each frame was measured carefully in the vicinity of the expected position using a Perkin-Elmer PDS 1010M microdensitometer, producing a digitized data base with a position resolution of 30″. Image processing software was used to superpose the frames from any one given scan, shifting the frames in the scan direction by an amount determined by the scan rate and the frame times. As a result a clear image of Algol could be obtained for all the Perseus scan sequences. The separation of the view axis from Algol at all times was now known, and by assuming that the scan orientations were as planned a complete attitude solution could be obtained. Figure 7 shows Perseus cluster scan sequences during the Perseus mission. In order to estimate the uncertainty in the result, we fitted the X-ray signal from each scan, illustrated in Figure 8a, with a model consisting of two Gaussian distributions representing

the emission from the cooling flow in the immediate vicinity of the active galaxy NGC1275 and the more extended cluster emission. When all scans were considered simultaneously in the fit, a 90% confidence error circle could be drawn for the center of each component, as shown in Figure 8b. The position of NGC1275 lay within the error circle for the cooling-flow component, and from the discrepancy we estimated that the 90% confidence error in the aspect solution was less than 0.8′. Comparing on each scan the predicted position of NGC1275 with the position of the center of the cooling-flow component, we obtained differences which have an average of 0.5′, and which had a standard deviation of 0.4′.

4 Construction, Operation and Calibration of the X-ray Detectors

4.1 The X-ray Proportional Counters

The two proportional counters, one of which is shown in Figure 9a, were refurbished after four Aerobee sounding rocket flights. They are 'multi-wire', constant-flow proportional counters equipped with a thin window of Mylar, which is 2.5 μ thick and coated on the inside with 30 Å of nichrome. The counting gas was P-10 (90% CH_4 and 10% Ar), stored at 1800 psia in a stainless steel bottle of volume 3.7 liter. The gas was regulated to 16.0 psia and flowed through the counter at 10 cm^3 min^{-1}. The counter X-ray aperture (25 cm $\times$ 60 cm) is filled with a block of aluminum honeycomb which supports the Mylar window and provides X-ray collimation (3° FWHM) in the direction perpendicular to the scan direction. After allowing for all mechanical obstructions in front of the detector window, we calculate the effective area of each detector aperture to be 660 cm^2. The calculated quantum efficiency of the detectors is shown in Figure 10 as a function of photon energy. It includes absorption by a second Mylar window, also 2.5 μ thick, placed in front of the fine collimators to act as a heat shield. This window was coated on the inside with 800 Å of aluminum and on the outside with 200 Å of SiO_x, which inhibited erosion during the flight by atomic oxygen.

The detector interior (Figure 9b) contains an array of wires which provides two layers of nine 2.8 cm square cells, each containing one anode wire running the length of the counter. In addition, an anode wire runs around the periphery of the array as part of the cosmic-ray veto system. The electronics is designed to accept primarily X-ray events, which arise in one cell only. Events registered in two or more wires by a cosmic-ray track are vetoed with an efficiency of 99% in orbit. The rate of these events, the 'coincidence count-rate', is measured continuously. The high voltage ($\sim$2950 V) on the anode wires is adjusted continuously to stabilise the gain, using a feed-back loop which monitors the pulse-height distribution of X-ray events in a small separate proportional counter. This shares the main counter gas flow and is made to count at a fixed mean rate by a 10 μCi radioactive source ($^{55}Fe \rightarrow {}^{55}Mn + \gamma$) of 5.898 keV ($^{55}Mn$ $K_{\alpha 1}$) X-rays.

The electronics amplifies the anode signals, vetoes particle events, and sorts the remaining events into a pulse height spectrum. The accepted events are digitized and sorted into 128

pulse height channels. Events in these channels are accumulated for 0.8192 s, equivalent to two periods of the major frame of the payload pulse code modulated (PCM) data storage system, and then the accumulated spectrum is shifted to a buffer to be read by the PCM encoder. The spectrum of each layer of each detector is accumulated and stored separately.

A solenoid driven ^{55}Fe calibration source is moved into the detector aperture once per orbit, as described in §2 and in Figure 3. A typical pulse height spectrum of the calibration source is shown in Figure 11. Two Gaussian functions have been fitted to the main peak and the escape peak, and Figure 12 shows how the channel number of each peak, a measure of the detector gain, drifted slowly during the mission, probably the result of a slow rise in the payload temperature. The thermal control system had a wide deadband (10°–40° C) and a significant temperature change was observed over a period of two days. Using these calibrations the gain drift could be taken into account during the spectral analysis of the X-ray events.

Pre-flight and in-flight measurements of the detector resolution are summarized in Table 2, which reveals no significant difference between ground and flight operation. The detector calibration source measures local resolution only, whereas the average over the detector aperture is required for scientific analysis. The average resolution was measured before flight in a vacuum chamber, using an ^{55}Fe source which was moved systematically across the detector aperture. The ratio of this result to the resolution measured when the flight calibration source was actuated in the laboratory has been applied to the flight calibrations to yield the in-flight average resolution listed on the bottom line of Table 2.

Fitting of the calibration spectra yielded also the intensity of the escape peak as a fraction of the main peak intensity, and the results are given in Table 3.

Prior to installation in the optical bench each detector was subjected to a vibration test using specifications determined by the measured conditions in the shuttle payload bay during launch, after which tests were performed in vacuum to verify that no change in the detector characteristics had occurred. In addition, each detector was operated during a thermal test in which the instrument temperature was varied over the range 0° to 50° C.

4.2 The X-ray Collimators

One of the four collimator modules which are mounted on the optical bench (Figure 2b) is shown in Figure 13. Inside a structure of AZ31B magnesium alloy are mounted 15 identical grids, each a molybdenum sheet 0.075 mm (0.003 in) thick. Into each sheet has been etched very precisely a regular array of 1 cm long slits 0.310 mm wide and spaced 0.485 mm apart. Before assembly of the collimator each grid was measured at six representative points using a scanning microscope, and this established that the grids had been etched with an accuracy of ± 7 μ (0.0003 in) rms. Each grid was then mounted in a flat frame, which in turn was mounted loosely in the collimator structure. To align the grids so that the slits in the 15 grids were accurately in register, the collimator was clamped onto a granite measuring table and the frames positioned using dial gauges which engaged reference edges on each grid. In this manner the grids could be positioned with an accuracy of 13 μ (0.0005 in). The final

Table 2. The energy resolution of the SPARTAN 1 detectors, expressed as a fraction of the energy of the ^{55}Fe peak (5.898 keV)

Time (sec)	Energy resolution (FWHM)			
	Detector 1		Detector 2	
	layer 1	layer 2	layer 1	layer 2
PRE-FLIGHT (1)				
(a)	0.163±0.001	0.174±0.003	0.163±0.002	0.167±0.003
(b)	0.171±0.001	0.173±0.002	0.179±0.002	0.177±0.002
INFLIGHT (1,2)				
(a)	0.162±0.003	0.168±0.006	0.165±0.003	0.171±0.007
(b)	0.170±0.004	0.168±0.008	0.180±0.005	0.181±0.009

NOTES

1. The two lines (a) and (b) designate two different measurements: (a) Using the flight calibration source. (b) Scanning a laboratory cource uniformly across the aperture.
2. The overall resolution of the detector inflight, when the aperture was uniformly illuminated, was obtained by correcting the resolution obtained from the calibration line. This was done using the results of the ground calibrations.

Table 3. The intensity of the calibration source escape peak at 2.957 keV, expressed as a fraction of the main peak at 5.898 keV.

Detector 1		Detector 2	
layer 1	layer 2	layer 1	layer 2
0.037±0.004	0.044±0.007	0.039±0.004	0.032±0.008

step was to clamp the 15 frames firmly in the structure by tightening an array of bolts. The alignment of the grids was later verified at the Los Alamos National Laboratory (LANL), prior to the X-ray calibration of each collimator, by sighting each grid with a special travelling microscope inserted between the frames.

The collimators were tested and calibrated at LANL in a vacuum tank equipped with an electron bombardment X-ray source capable of producing a parallel beam with a width of about 10 cm. The divergence of the beam was $\pm 10''$. An aluminum target was used in the source, producing a beam of Al K (1.49 keV) X-rays. A mask was inserted in front of the source in order to define a square beam of width 1 in, which illuminated an area centered between the structural support bars (Figures 2b & 13). The beam intensity was calibrated, so that by measuring the intensity with a special proportional counter detector mounted behind the collimator the transmission could be measured, and by rotating the collimator in the chamber the angular response function could be measured. The angle between the beam and the collimator view axis was varied over a wide range ($\pm 3°$), in order to search for side-lobes of the collimator response. The measurements indicated that any such leaks were negligible. Calibration of the primary response revealed a slightly bell-shaped response, due to imperfections in assembly, rather than the expected triangular shape. The full width at half maximum (FWHM) of the response function was measured, as was the peak transmission efficiency, and both were close to the design values. The transmission of the collimators to a source on-axis was 55%. A harsh thermal test was made, in which a plate cooled to 80° K covered the aperture. The plate, close to but not touching the collimator, contained a square aperture of width 1 in to admit the X-ray beam. No measurable influence upon the shape of the response function or the peak efficiency was measured. In flight, thermal protection was provided by an aperture heat shield (§4.1) and by a multilayer insulation blanket mounted on each side of each collimator (Figure 2b). Vibration tests of the collimators were made, using the same specifications as used for the proportional counters, followed by X-ray tests to verify that no degradation of the response function had occurred.

The final calibration of the response function was performed in orbit, as described in §2 and §3, to compensate for a number of possible effects:

- misalignment of the two modules mounted on each detector;
- small shifts in the grid alignment caused by the launch acoustic and vibration environment in the orbiter bay; and
- changes induced by the thermal conditions in space.

No such effects were detected as a result of analyzing the data obtained during the calibration. Figure 14 shows the count-rate of each detector during the transit of the strong stellar X-ray source Sco X-2. A satisfactory fit to the data was obtained using a model of the response function in which the variation with distance from the peak is a quartic polynomial. The measured width (FWHM) was $5.5'$ for detector 1 and $5.8'$ arcmin for detector 2. The fitting procedure also yielded the time at which the X-ray count-rate was a maximum, which could be combined with the known position of Sco X-2 and the startracker aspect solution to yield

Table 4. Preflight and inflight calibration of the offsets between the startracker and each of the two detector view axes. The offsets are measured in the direction along the scan track.

	startracker arcmin	X-ray detector 1 arcmin	X-ray detector 2 arcmin
Preflight	0	1.27±0.32	2.47±0.29
Inflight	0	1.98±0.50	2.66±0.50

the offsets in the scan direction between the X-ray axes and the startracker axis. The values are given in Table 4, where they are compared with the values measured before launch.

5 Determination of the Detector Background

The upper plot in Figure 15 shows the X-ray count-rate of detector 2 from the time it was switched on until the payload was shut down 17^h 32^m after deployment by the orbiter. As described by Cruddace et al. (1990), this shutdown was premature and was caused by exhaustion of the ACS gas supply, the result of excessive noise in the rate-gyro signal and consequent increase in activity of the ACS gas jets. However, about 60% of the observations were completed. Careful scrutiny of Figure 15 reveals the sequence of operations repeated every orbit. For example the strong, sharp spike, repeated every 90 minutes approximately, is the X-ray calibation, and between adjacent spikes appear the X-ray signals recorded during the observation of first the Perseus cluster and then the Galactic center.

The lower plot in Figure 15 shows the coincidence count-rate, which is a measure of the intensity of the flux of high-energy particles encountered by SPARTAN 1 in its orbit. Between 3 and 8 hours after deployment this count-rate distribution is interrupted three times, and Figure 15 shows a sharp rise preceding each interruption. This heralded the entry of SPARTAN 1 into the South Atlantic Anomaly, when the particle flux rose sharply, causing the coincidence count-rate to exceed a preset threshold in the detector electronics, which commanded a shut-down of the high-voltage supply. This was a safety feature designed to avoid circumstances in which proportional counter performance can be permanently degraded by sustained high counting rates. The detector high-voltage supply was switched back on automatically after 5 minutes, but was switched off soon thereafter if the particle flux was still too high. In both the upper and lower plots of Figure 15 two or three such restarts may be discerned. The large oscillations in the coincidence count-rate between 12 and 17 hours after deployment occurred twice per orbit, and corresponded with times when SPARTAN 1 encountered regions at high geomagnetic latitude, where the particle flux rises substantially from the levels found in equatorial regions.

These large variations in the particle-flux encountered during the mission caused significant changes in the background count-rate of the detectors, namely in the events remaining

after all vetoes had been applied (§4.1). This had to be taken into account during the observations. For example, in Figure 16 we show the detector count-rate during one complete sequence of scans over the Perseus cluster. At the points where the count-rate is lowest the X-ray collimator is pointed in a direction almost one degree away from the cluster center, yet even here the weak flux from this outer region of the cluster can be detected. To deduce this with the required precision, the background due to particles has to be measured and subtracted. This was done by correlating the coincidence count-rate with the detector background rate, at times in the mission when no X-ray source was being observed. Then during an observation this correlation and the coincidence count-rate were used to derive the background rate. In Figure 17 we show this correlation, which was derived using data taken while the pointing direction was within 10° of the cluster center. This restriction was a precaution, as there is no *a priori* reason to suppose that a unique correlation is obtained which applies to all particle environments encountered by SPARTAN 1 in its orbit around the Earth.

References

Cruddace, R. G., Brandenstein, D. C., Creighton, J. O., Fabian, J. M., Fenimore, E. E., Fritz, G. G., Gross, C., Gutschewski, G., Lucid, S. W., Nagel, S. R., Shrewsberry, D. J., and Zimmermann, D. 1990, Journal of the British Interplanetary Society, **43**, 223

Figure 1. The free-flying payload SPARTAN 1 shortly after release from the orbiter Discovery (STS 51G) on 20 June 1985. The front half of the payload, displaying the mission decal, is a large sunshade for the instrument.

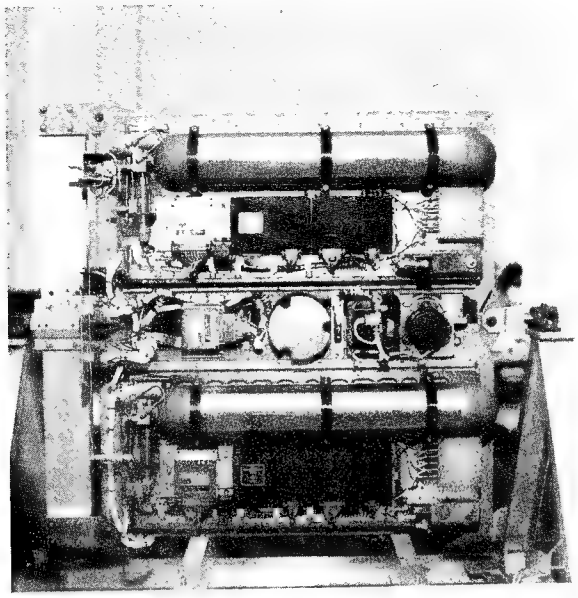

(a)

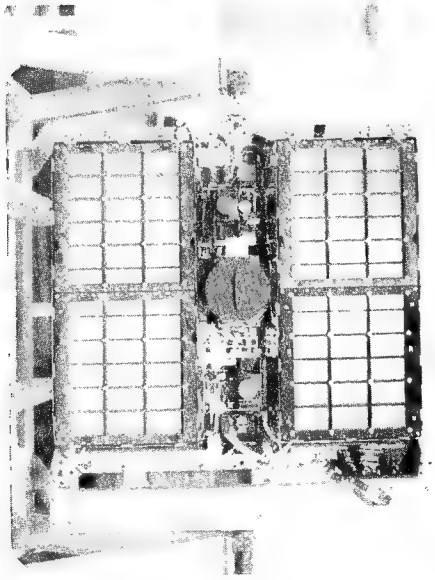

(b)

Figure 2. Two views of the SPARTAN 1 'optical bench', upon which were mounted two X-ray proportional counters equipped with fine collimators, two 35 mm aspect cameras, a startracker, and the rate-gyros of the attitude control system. View (a) shows the rear sides of the two counters; between them is the startracker (center) and the rate-gyros (right). View (b) shows the fine collimators; between the two collimator banks are situated the startracker and the two 35 mm cameras.

OBSERVING SEQUENCE FOR ONE ORBIT

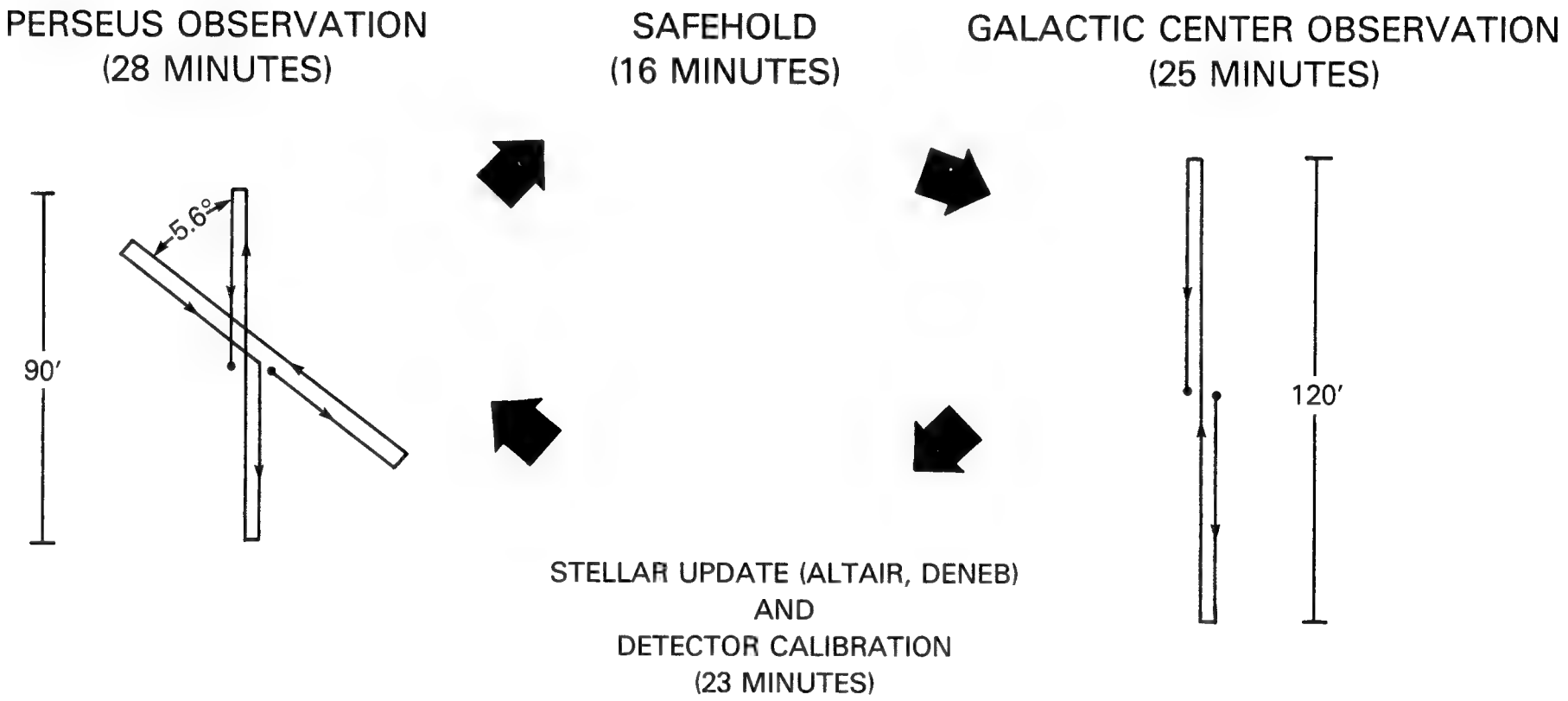

Figure 3. A summary of the sequence of maneuvers performed by SPARTAN 1 each orbit. The stellar update was performed in order to remove gyro drift errors. The safehold position was held when the astronomical sources were inaccessible, and an orientation had to be selected to avoid the startracker viewing the sunlit Earth.

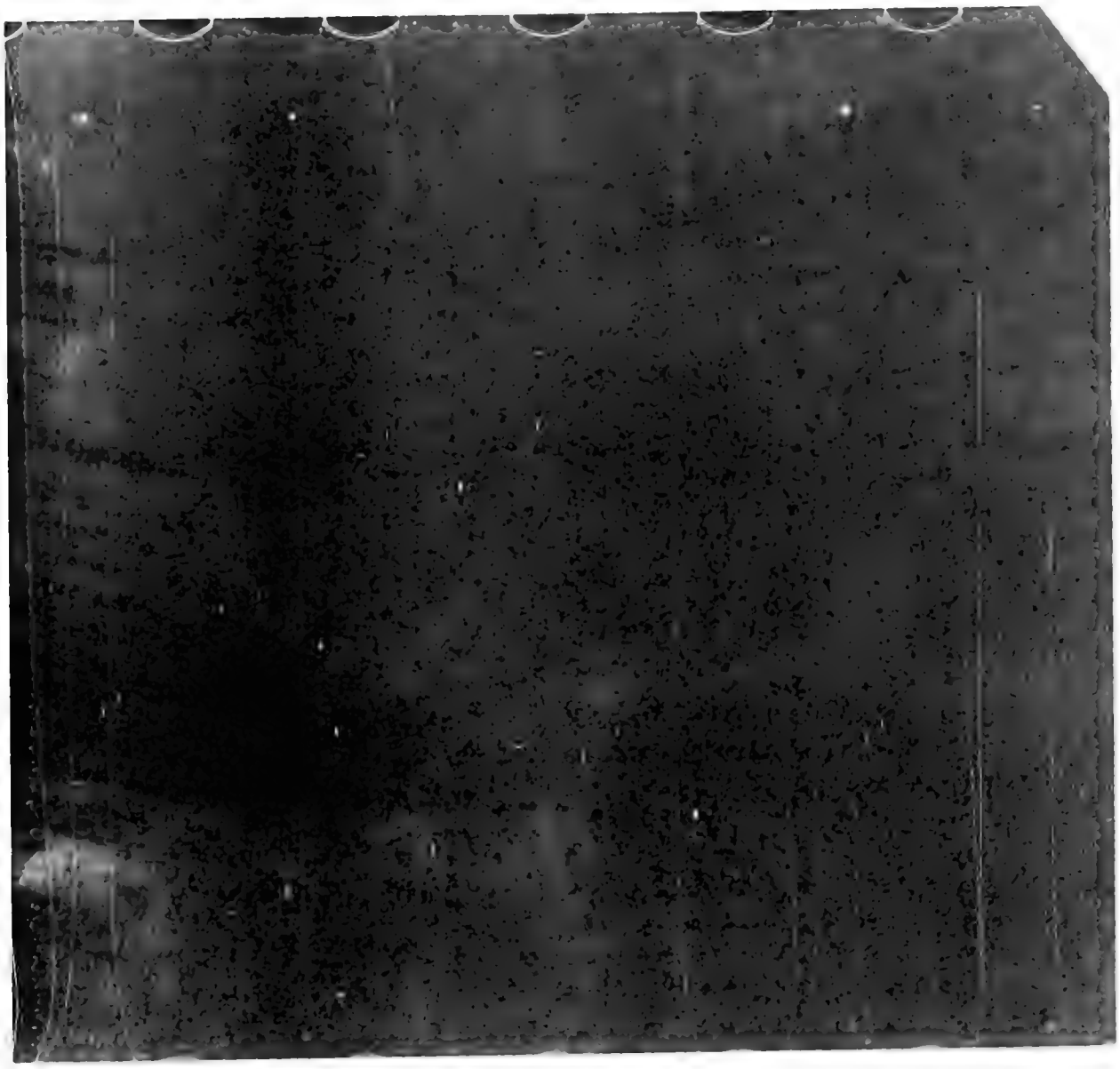

Figure 4. A print of one 10 second exposure made by one of the two SPARTAN 1 35 mm aspect cameras during a slow scan across the Galactic center. Fiducial lights are visible near each corner. The long streaks are cracks in the emulsion due to exposure to vacuum.

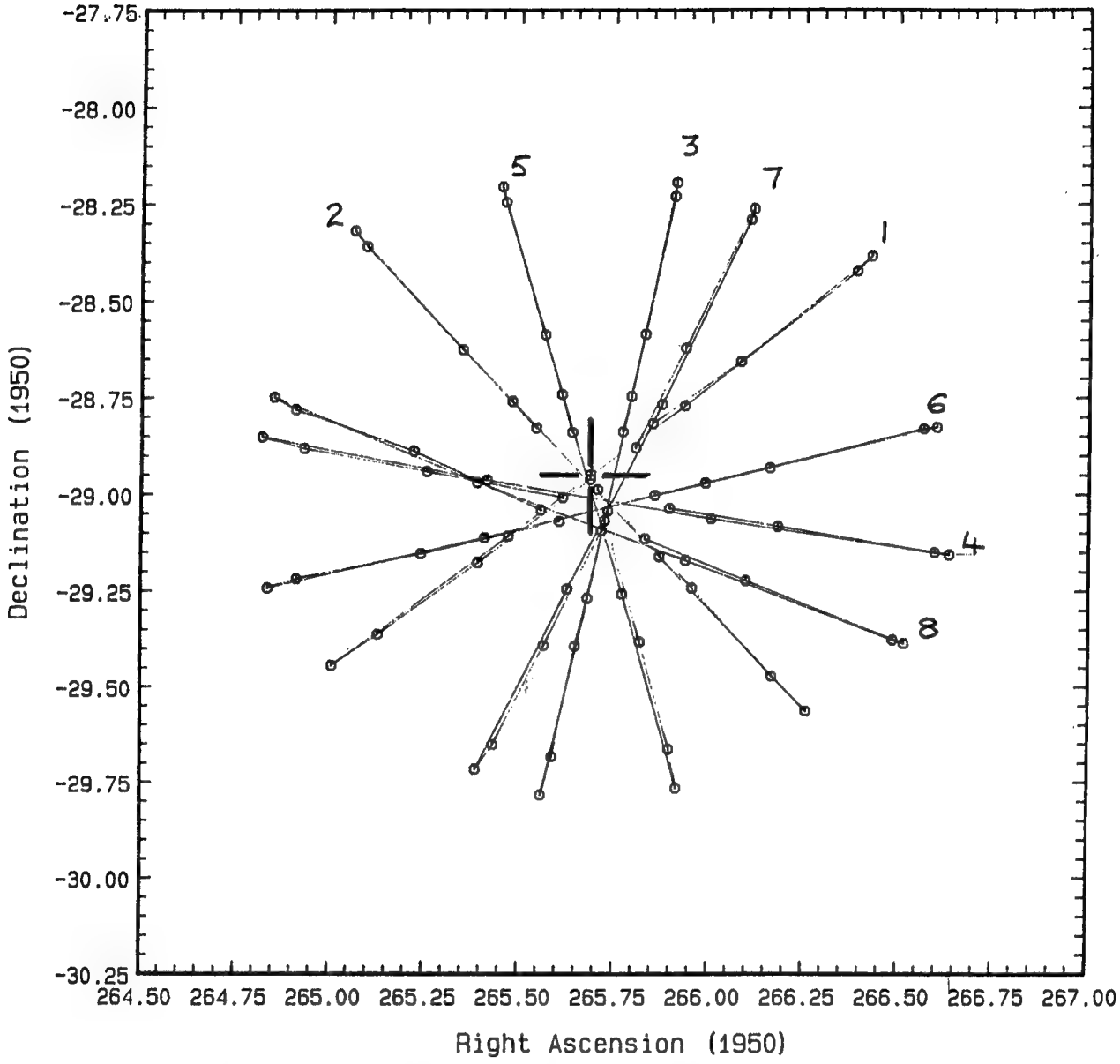

Figure 5. A map of the scans of the Galactic Center made during the SPARTAN 1 mission. Eight of the 14 planned scan sequences were made before the mission was terminated prematurely.

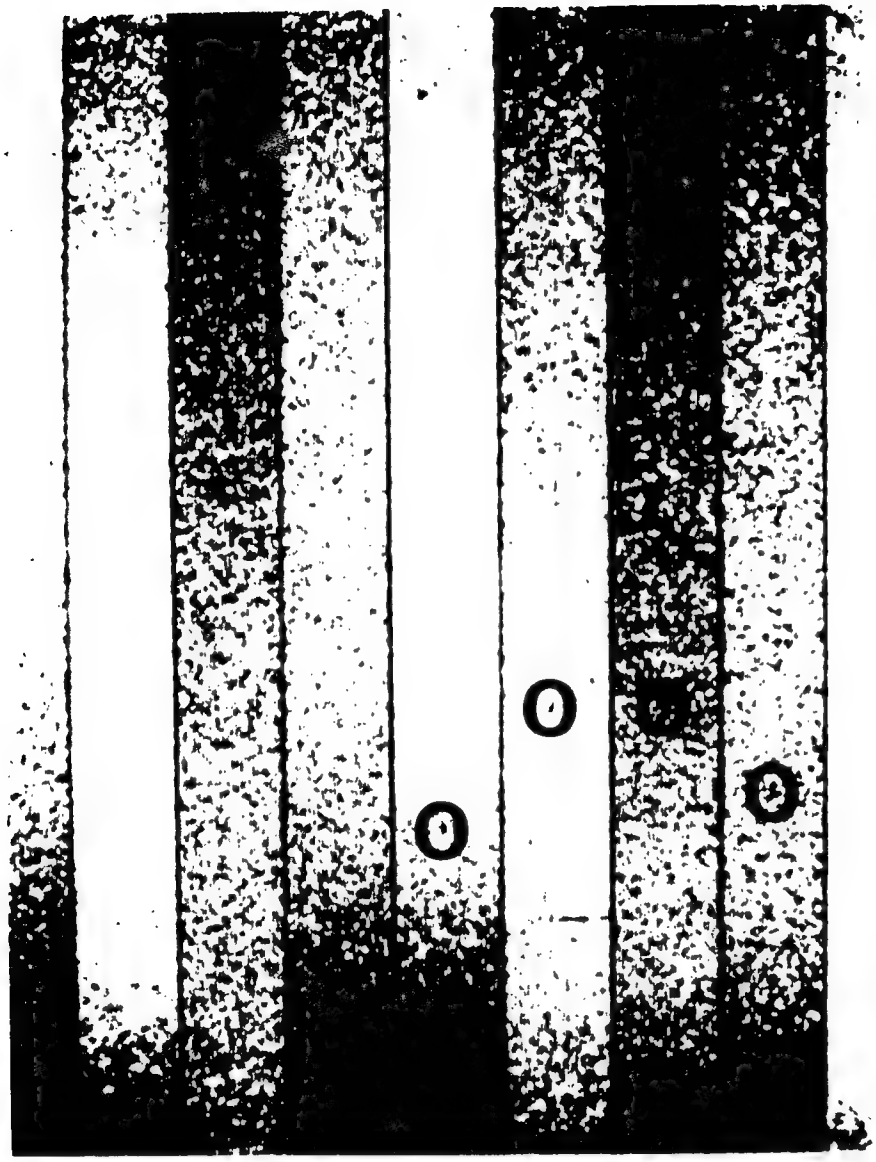

Figure 6. Despite protection by sunshades the aspect camera film was fogged by scattered solar light during the SPARTAN 1 scans across the Perseus cluster. We show here slices taken from a sequence of seven frames. In spite of the fogging, the star Algol could be found on the film, sometimes by eye as shown here and in other scans by means of microdensitometry of the film. With this information an accurate aspect solution was recovered.

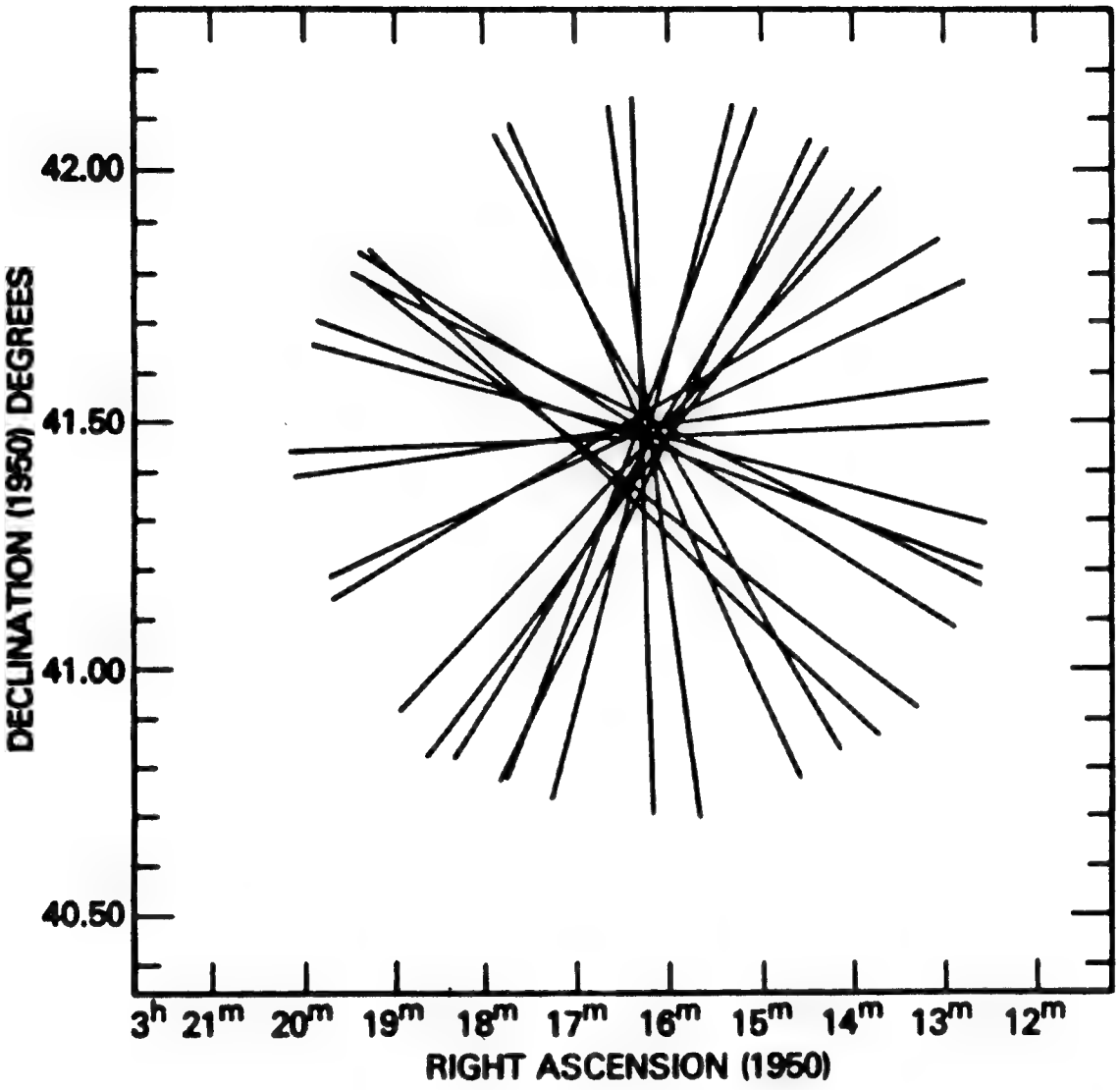

Figure 7. A map of the scans of the Perseus cluster made during the SPARTAN 1 mission. Ten of the sixteen planned scan sequences were made before the mission was terminated prematurely.

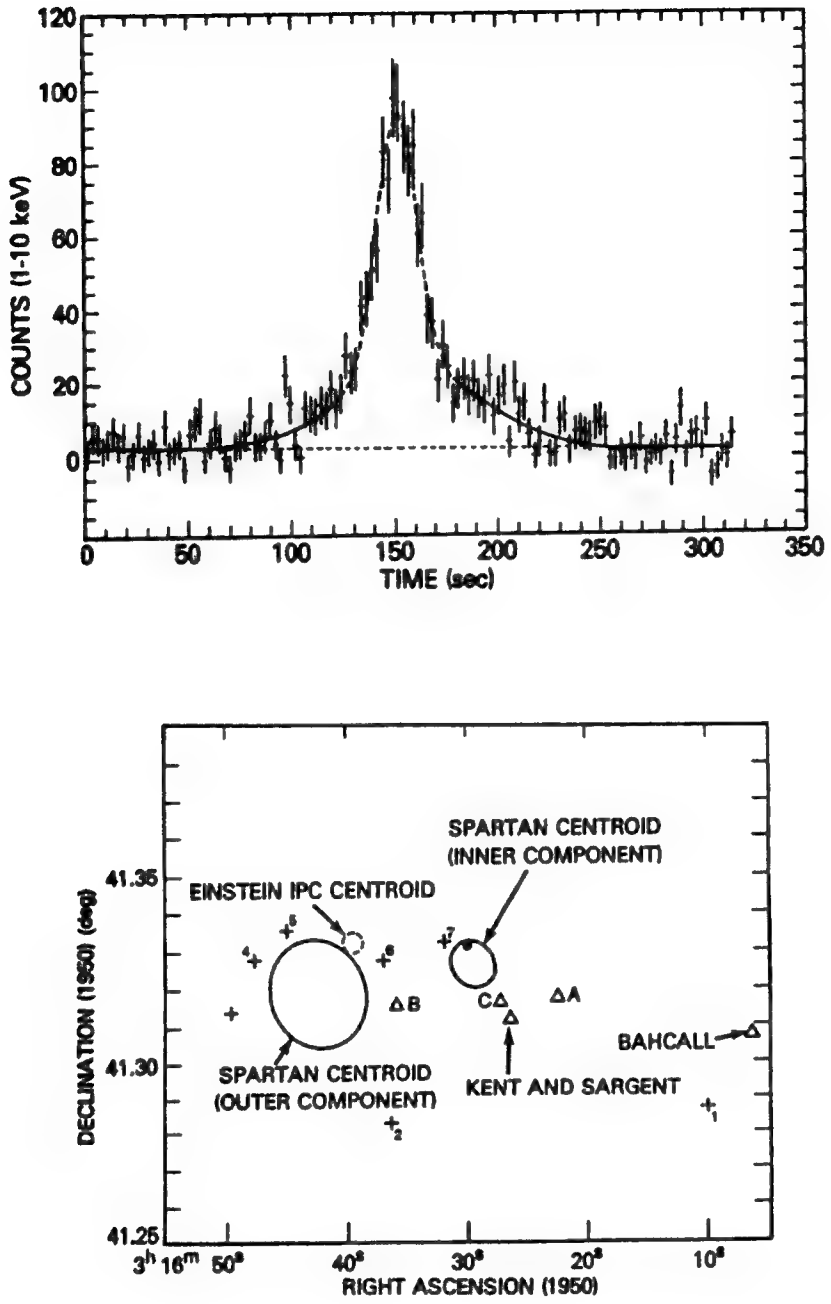

Figure 8. (a) A histogram of the counts recorded during a scan of the Perseus cluster. The two components of the emission, the central cooling flow and a more extended emission, are represented by the two best fit Gaussian functions. (b) The error ellipses for the centers of the two emission components, on the left for the cooling flow and on the right for the extended emission. The black dot in the smaller circle is the optical position of the active galaxy NGC 1275, which lies at the core of the cooling flow.

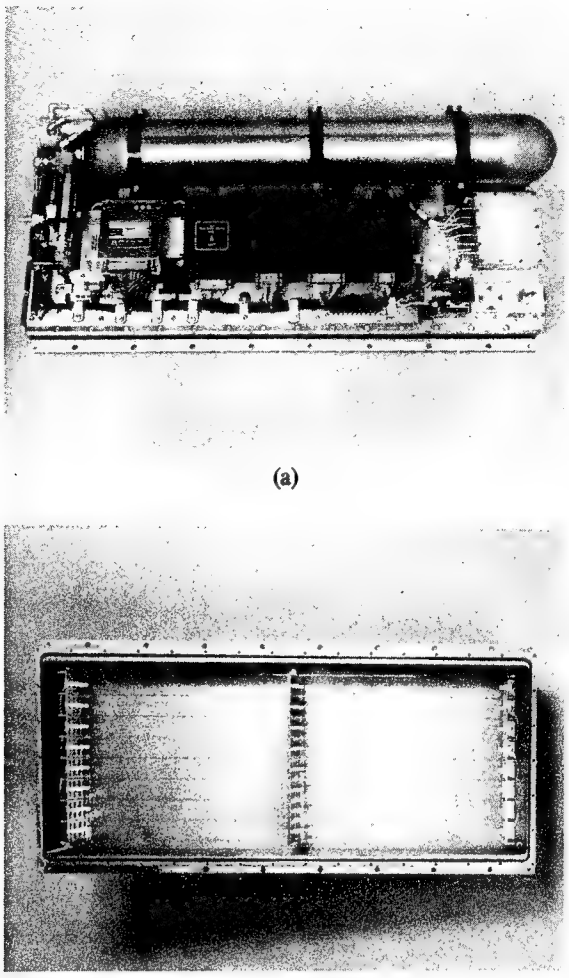

(a)

(b)

Figure 9. Two views of the SPARTAN 1 proportional counter. (a) Exterior view of the rear of the counter showing the P-10 gas supply and pressure regulation system and the data, power, and high voltage systems. (b) A view of the counter interior showing the array of high voltage and ground wires. The array forms two layers of nine 60 cm long cells of square (2.8 cm) cross section, each cell containing one high voltage wire running along its axis.

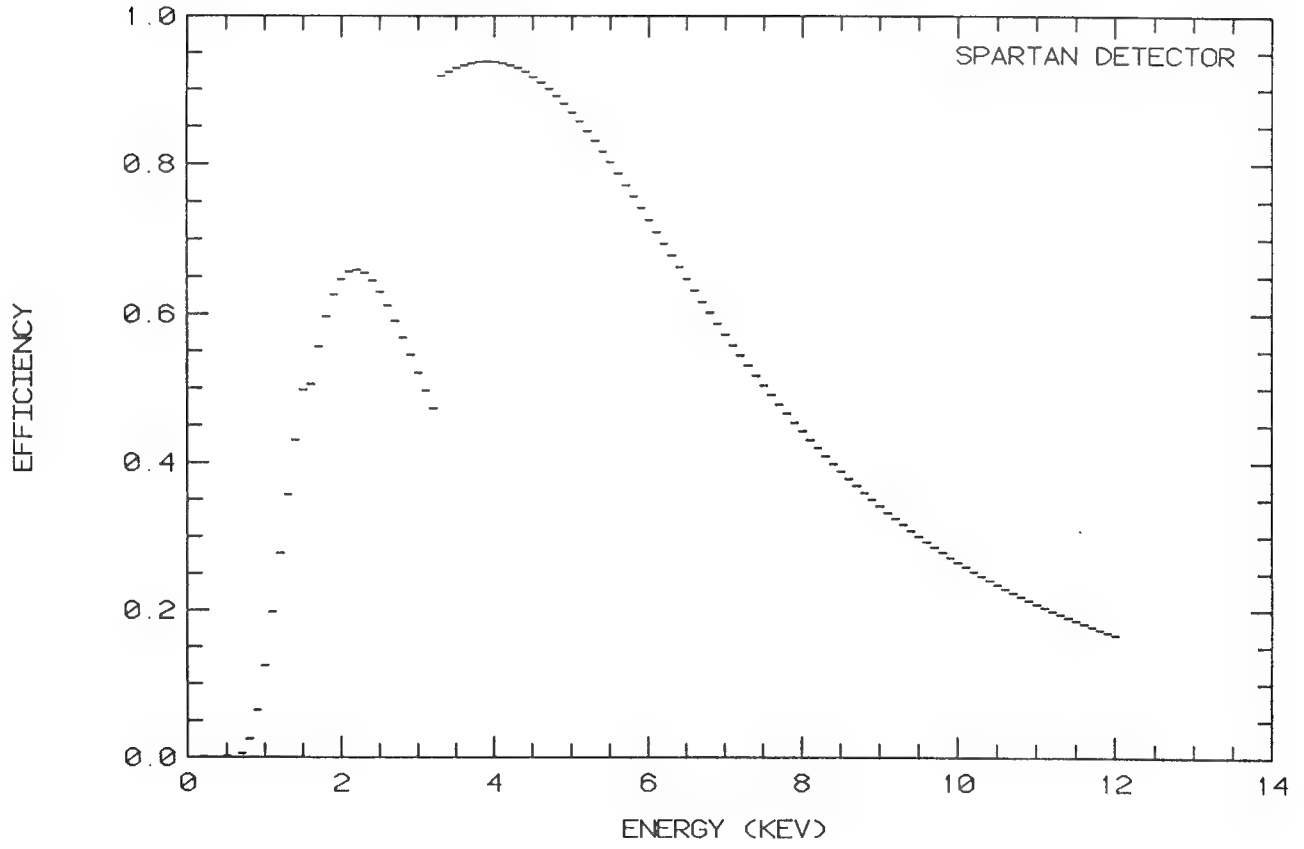

Figure 10. The quantum efficiency of the SPARTAN 1 detectors, plotted as a function of the incident photon energy.

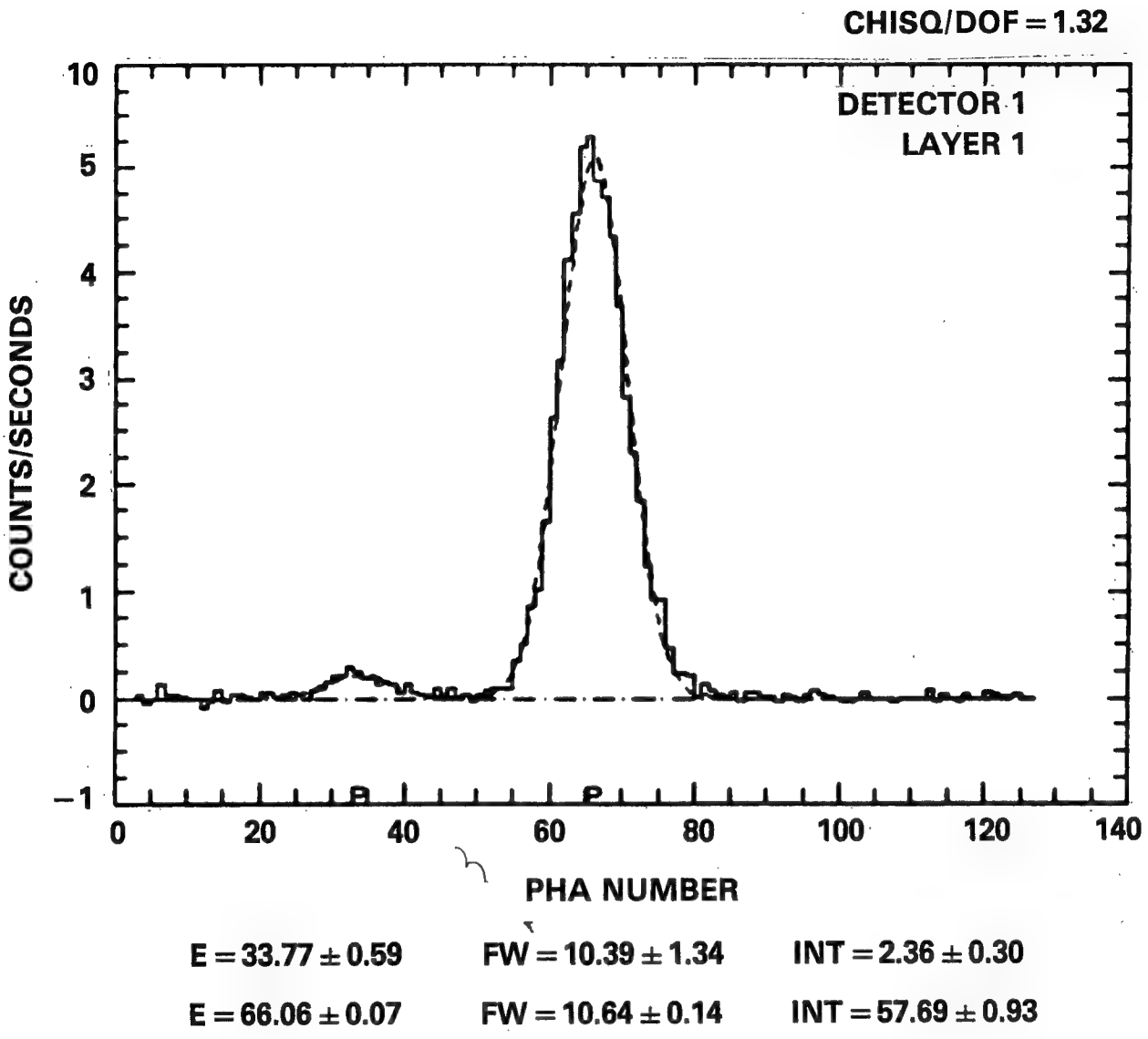

Figure 11. The pulse height spectrum of one detector when the ^{55}Fe calibration source shone into the aperture.

SPARTAN-1 ENERGY CALIBRATION

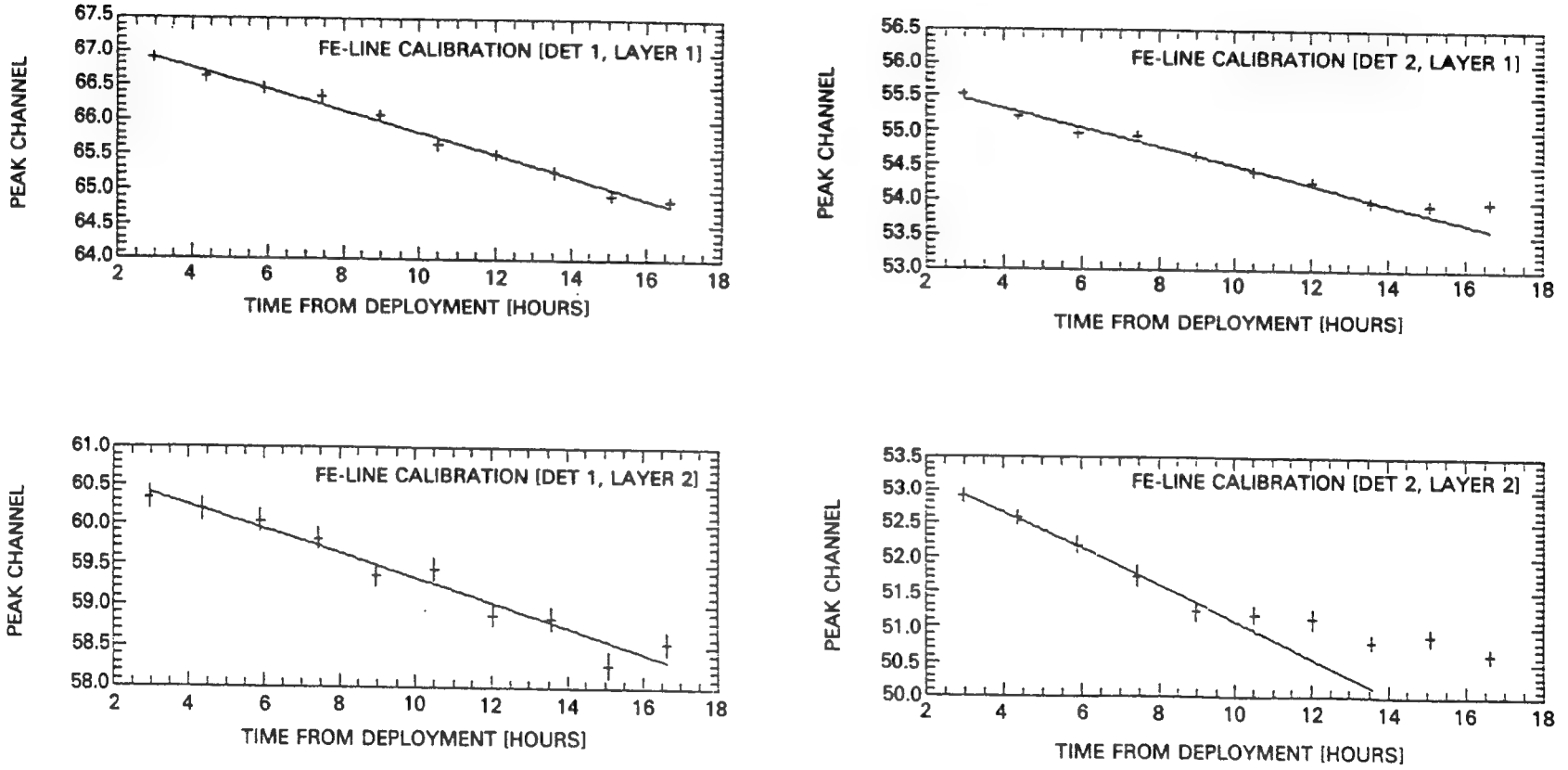

Figure 12. The pulse height channel of the peak of the ^{55}Fe calibration line, plotted as a function of elapsed mission time. The slow drift in gain in each layer of the two detectors is evident. It was caused by a gradual rise in the payload temperature.

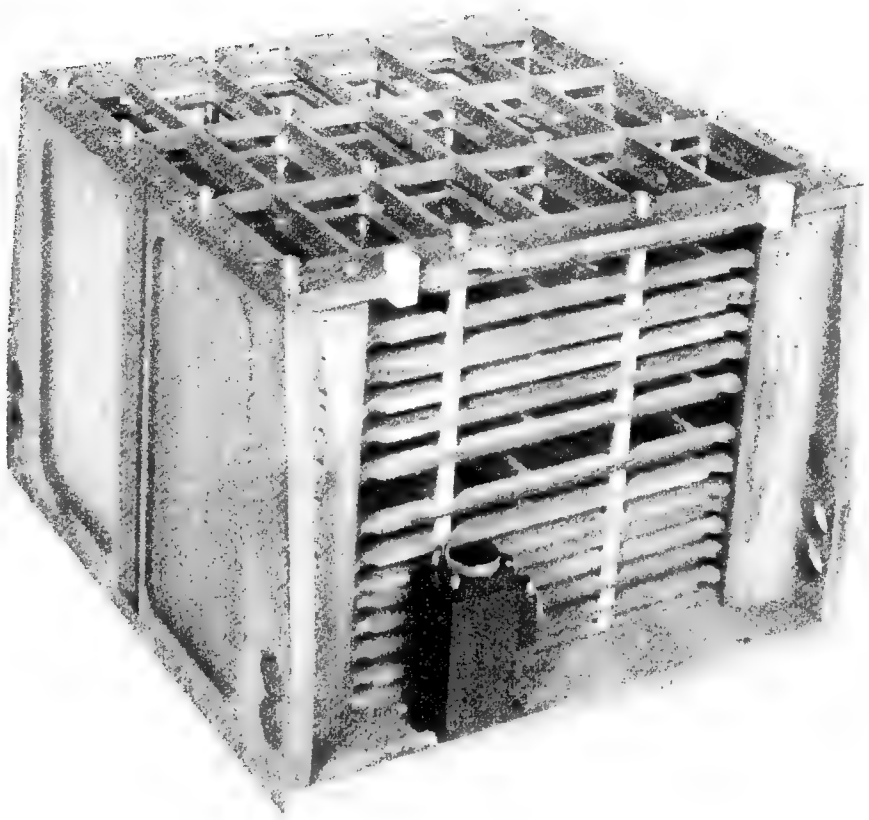

Figure 13. A view of one of the four collimator modules. Each detector was equipped with two co-aligned modules. The structure contains 15 thin molybdenum sheets, which have been etched to produce an array of fine slits. The sheets are accurately spaced and registered so as to provide a slit-like field of view 5 arcminutes wide (full width at half maximum).

SCO X-2 TRANSIT

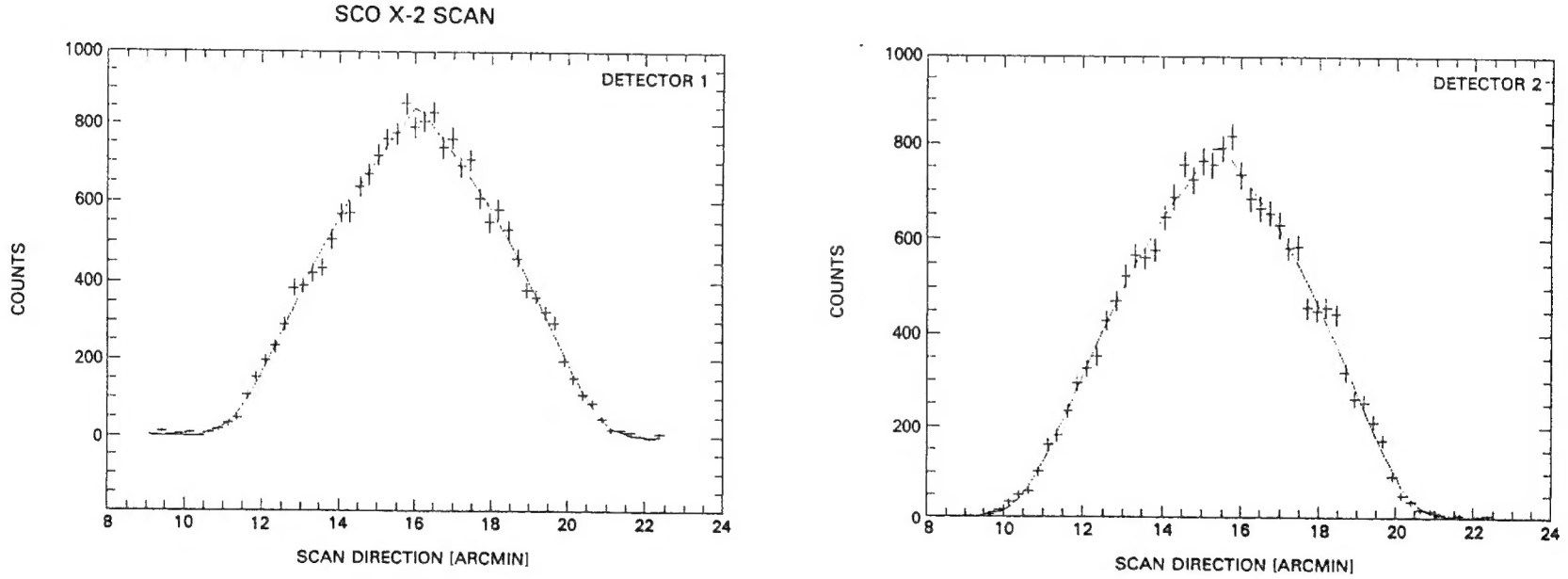

Figure 14. The count rates in each detector during a slow scan across the stellar X-ray source Sco X-2 (1H1702-363). This in-flight calibration of the collimator response function revealed a slightly bell shaped distribution, in contrast to the triangular response of a perfect collimator.

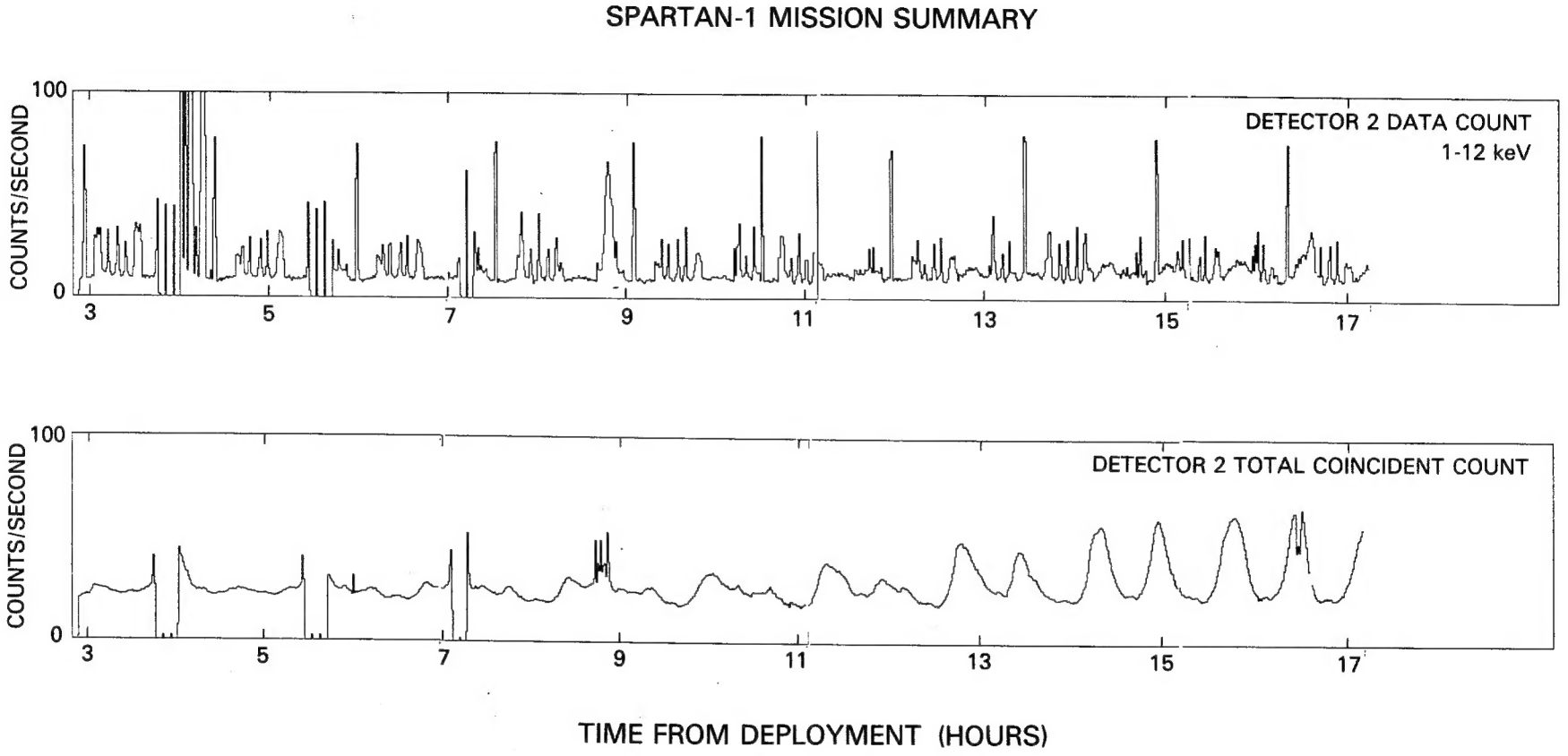

Figure 15. Two histograms of events recorded by one detector during the whole observing phase of the SPARTAN 1 mission. The upper plot shows the X-ray response of the detector, while the lower plot follows the rate at which vetoed events are counted.

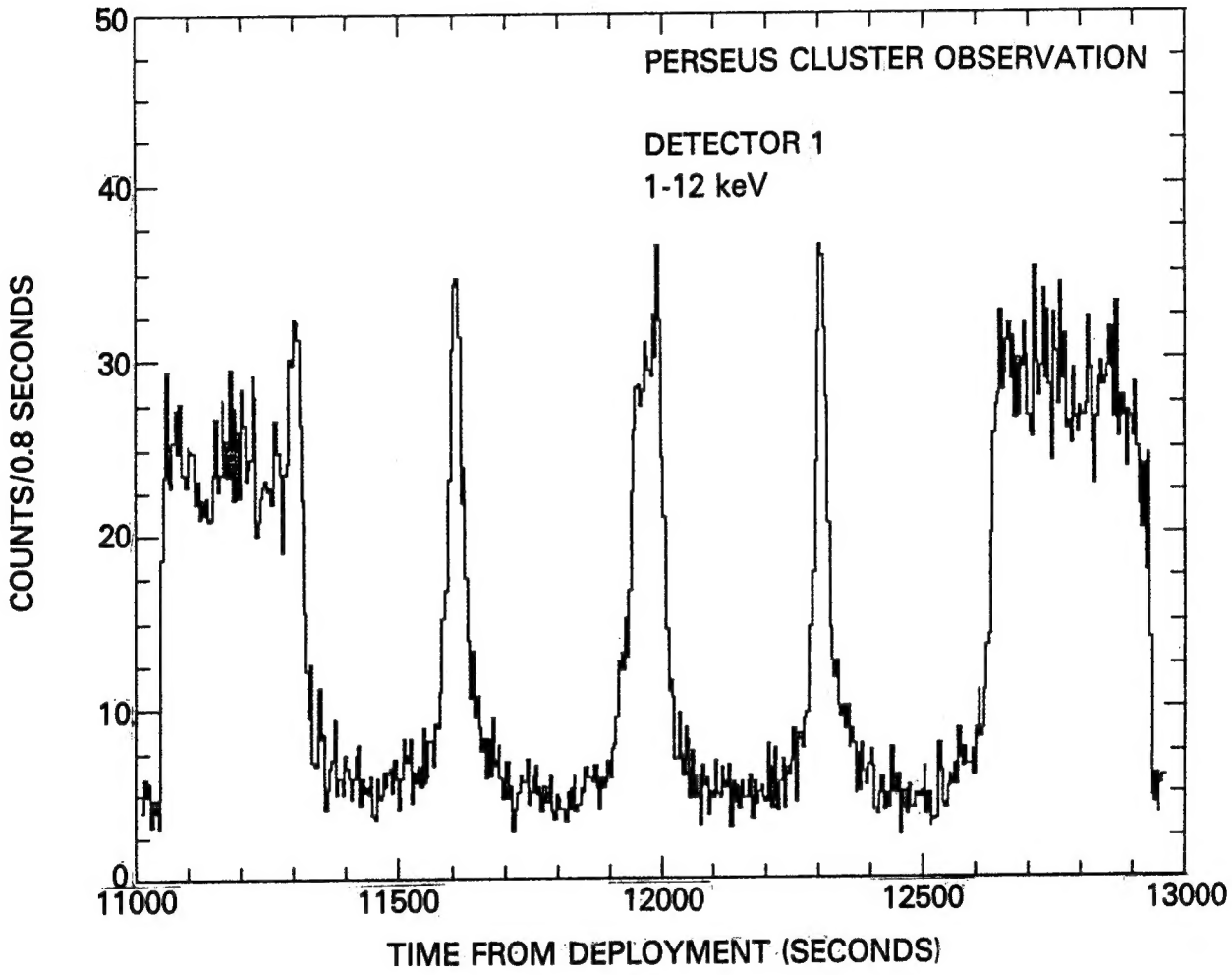

Figure 16. The X-ray count rate of one detector during one sequence of scans over the Perseus cluster. A large steady signal is recorded at the end of each scan, as the collimator remains pointed at the cluster center (see Figure 3).

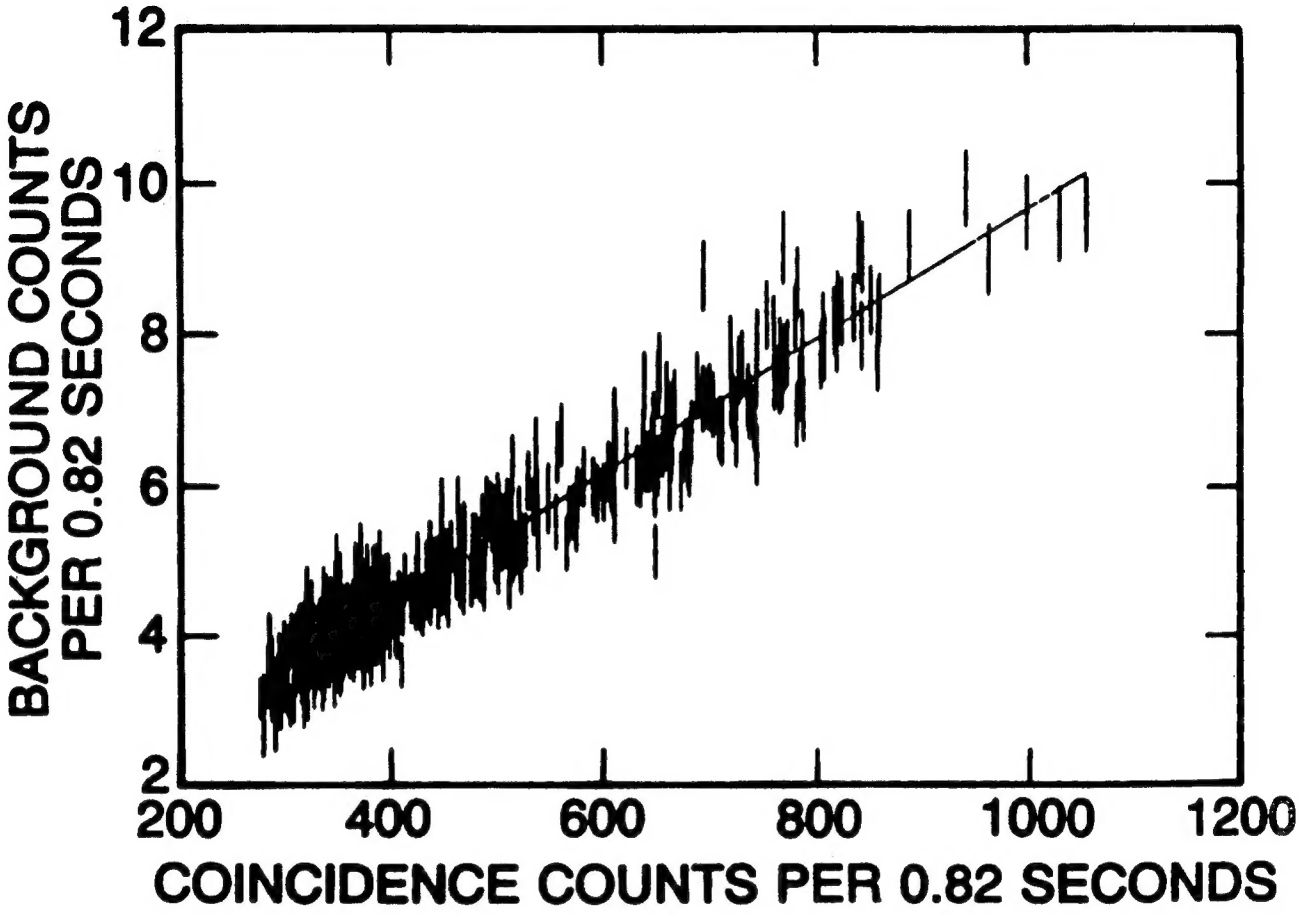

Figure 17. A correlation between the detector background count rate after vetoing of cosmic ray events and the detector coincidence (vetoed events) count rate. This correlation was established using data well removed from the Perseus cluster and then used to estimate background during each scan over the cluster.